Planar isotropy of passive scalar turbulent mixing with a mean perpendicular gradient

L. Danaila,[1] J. Dusek,[2] P. Le Gal,[1] F. Anselmet,[1] C. Brun,[3] and A. Pumir[3]
[1]*IRPHE, 12 Avenue du Général Leclerc, 13003 Marseille, France*
[2]*IMF, 2 rue Boussingault, 67000 Strasbourg, France*
[3] *INLN, 1361 route des Lucioles, 06560 Valbonne, France*
(Received 16 October 1998; revised manuscript received 23 March 1999)

A recently proposed evolution equation [Vaienti *et al.*, Physica D **85**, 405 (1994)] for the probability density functions (PDF's) of turbulent passive scalar increments obtained under the assumptions of fully three-dimensional homogeneity and isotropy is submitted to validation using direct numerical simulation (DNS) results of the mixing of a passive scalar with a nonzero mean gradient by a homogeneous and isotropic turbulent velocity field. It is shown that this approach leads to a quantitatively correct balance between the different terms of the equation, in a plane perpendicular to the mean gradient, at small scales and at large Péclet number. A weaker assumption of homogeneity and isotropy restricted to the plane normal to the mean gradient is then considered to derive an equation describing the evolution of the PDF's as a function of the spatial scale and the scalar increments. A very good agreement between the theory and the DNS data is obtained at all scales. As a particular case of the theory, we derive a generalized form for the well-known Yaglom equation (the isotropic relation between the second-order moments for temperature increments and the third-order velocity-temperature mixed moments). This approach allows us to determine quantitatively how the integral scale properties influence the properties of mixing throughout the whole range of scales. In the simple configuration considered here, the PDF's of the scalar increments perpendicular to the mean gradient can be theoretically described once the sources of inhomogeneity and anisotropy at large scales are correctly taken into account. [S1063-651X(99)02108-X]

PACS number(s): 47.27.Gs, 47.27.Ak, 47.27.Eq

I. INTRODUCTION

Understanding the statistical and dynamical properties of high Reynolds number turbulent flows is currently the subject of many investigations. Kolmogorov theory ([1], hereafter referred to as K41), has provided some major insight in this field. It assumes local isotropy in high Reynolds number turbulent flows. The K41 theory successfully predicts the structure of the two-point correlation function of the velocity field in the inertial range, intermediate between the large anisotropic scales, where energy injection takes place, and the small scales, where viscosity is important. Local isotropy for the inertial range signifies simply that all the statistical properties of the field are invariant under any rotation direction. In particular, this property implies the independence of these scales with respect to the large scale forcing, in general anisotropic and very specific (nonuniversal). The K41 theory leads to a scaling law for the velocity increments, $S_p = \langle (u(r)-u(0))^p \rangle \approx \overline{\epsilon}^{p/3} r^{p/3}$, when the separation r is in the inertial range, and where $\overline{\epsilon}$ is the mean dissipation rate. Accordingly, these moments should generally determine self-similar probability density functions (PDF's).

The K41 theory, originally derived for the velocity field was later naturally extended to the passive scalar field, by Oboukhov [2] and Corrsin [3]. Indeed, it was reasonable to argue that the passive scalar properties would be completely determined by the driving field behavior.

Significant deviations of the high order velocity moments from the K41 predictions were found experimentally [4]. Understanding these deviations, attributed to the phenomenon called ''intermittency,'' and predicting the corresponding anomalous scaling laws, has become a major challenge. Several ''phenomenological models,'' from the Kolmogorov model (K41) to the refined similarity hypothesis (RSH) [5], or the multifractal model [6], tried, with more or less success, to refine the predictions qualitatively and quantitatively for the velocity scaling law exponents (see Ref. [7] for a recent review). Recently, a general analysis of the turbulent cascade was proposed in Ref. [8]. A canonical distribution of velocity differences at any scale was introduced, with the help of a conserved quantity throughout the whole scale range. Several of the previously mentioned models can be recovered as particular cases in this general formulation. A phenomenological description of the statistical properties of the cascade was also presented in Ref. [9], providing an evolution equation for the probability density function of the velocity increment. A method to extract the exponents corresponding to the various irreducible representations of the rotation group was proposed in Ref. [10], therefore addressing the issue of isotropy in turbulent flows. Alternatively, in [11], anomalous scaling exponents for the dynamic field were obtained, by taking into account the interaction between random and large-scale coherent components of a turbulent field.

Generally speaking, the passive scalar field was found to exhibit a more anomalous behavior than the velocity field [12], being in this sense ''more intermittent than the velocity field.'' Specifically, the probability density functions (PDF's) associated with the inertial and dissipative scales deviate from self-similar behavior, and present wider than exponential tails more pronounced than those for the velocity field.

Several models have been proposed to explain passive scalar intermittency. Essentially, the models developed for the dynamic field were also ''translated'' for the passive scalar field. This implicitly supposes that the scalar field automatically inherits some properties from the advecting flow. Thus it is traditional to think that the passive scalar ''internal intermittency'' is due to the dissipation rate fluctuations for both kinetic energy and scalar variance [13,14]. Most theoretical models of internal intermittency are based on various assumptions for the dissipation rate variation through the scales. For instance, the RSH theory was adapted for the temperature field [15]. Alternatively, a lot of attention has been paid to analyzing, theoretically and phenomenologically, the anomalous scaling exponents of the temperature structure functions $S_{2n}(r)=\langle(\Delta\theta)^{2n}\rangle$ [16,17], with reasonable success.

A different approach to the problem was proposed by Kraichnan [18–20], who considered mixing by a Gaussian, white in time velocity field. The problem then reduces to a closed (Hopf) equation for the N-point correlation functions of the scalar [20,21]. A mathematical understanding of ''anomalous exponents'' has emerged from the study of these equations [22–24]. Anomalous scaling laws were effectively found for moments of order $N\geqslant 4$, and even for the third moment in the presence of a mean gradient [22,25]. Remarkably, a simple Gaussian velocity field (no intermittency) can induce an intermittent behavior of the passive scalar.

An alternative way to study intermittency effects is to investigate the PDF evolution through the scales. It is known that large–scale PDF's are in general Gaussian, when the boundaries direct influence is negligible. However, large-scale temperature increment PDF's are not always Gaussian. For instance, in Ref. [26] these PDF's were found to be sub-Gaussian (with a kurtosis equal to 2.3, smaller than the ''Gaussian'' value of 3), whereas, in Ref. [27], the large-scale PDF's were super-Gaussian. These results are due to different values of the ratio of the turbulent integral scale to the tunnel width (for the physics of this anomalous diffusion process, see Ref. [21]). The mixing we analyze in this paper presents a Gaussian large-scale temperature PDF.

The question is then to understand how exponential tails appear for the smaller scales, starting, for instance, from a Gaussian distribution at large scales. A new approach in this direction was developed in Ref. [28]. The basic objective is to develop a theory able to predict small-scale behavior of PDF's starting from their large-scale counterparts. The problem can be formulated as a partial differential equation in two variables—separation and passive scalar increment—involving two conditional expectations (of the velocity increment, and of the squared passive scalar gradient). These conditional expectations have either to be provided from experiments or direct numerical simulation (DNS), or to be modeled [29]. The basic weakness of this theory appeared to be the assumption of local three-dimensional (3D) isotropy for the passive scalar explicitly used in the derivation of Ref. [28]. The well-known Yaglom equation [30,31], relating the second-order moments to the third-order moments, of the temperature increments results from the PDF evolution equation.

The issue of validity of the 3D isotropy assumption has been addressed for different Reynolds numbers Re, and in different flow geometries. The flows used both in experiments (a slightly heated turbulent boundary layer and at the center of a von Kármán swirling flow, with an imposed temperature difference between the two disks) and in DNS (a homogeneous isotropic velocity field with a mean scalar gradient) show a significant degree of large-scale anisotropy, which may contaminate the small scales, whereas Ref. [28] assumes isotropy.

In the case of the von Kármán swirling flow, however, the temperature increment skewness in the center of the cell could be nearly zero, contrary to what generally happens in shear flows. This suggests that isotropy is a good approximation in this case, and it was indeed found that the theory developed in Ref. [28] is valid in a high Reynolds flow ($R_\lambda\approx 600$), over a significant subdomain of the inertial range [32]. In the case of the boundary layer, of the mixing by an homogeneous flow with a mean scalar gradient, or of the von Kármán swirling flow, only the PDF's in the plane perpendicular to this mean scalar gradient were analyzed. However, in the case of the boundary layer, PDF's and conditional averages are not symmetric, as they should be if the statistics were isotropic. They had in this case to be symmetrized, as a palliative for the 3D isotropy. With this procedure, it was found that the range of scales over which the theory of Ref. [28] applies (the ''validation domain''), includes the dissipative and small inertial scales [33], until limits which were found to be 50η [$\eta\equiv(\nu^3/\overline{\epsilon})^{1/4}$, is the Kolmogorov length scale] for a slightly heated boundary layer, with $R_\lambda=\lambda u'/\nu\approx 200$, or 30η in the DNS with a homogeneous isotropic velocity field and a mean temperature gradient, with $R_\lambda=82$ (where u' is the velocity rms, and λ is the Taylor microscale). Although the results of Ref. [33] are very encouraging, important questions regarding isotropy remain to be addressed. This question is particularly important, as most flows do exhibit a significant anisotropy.

Isotropy issues have been extensively studied in different flow configurations [34–39]. A quantitative characterization of isotropy turns out to depend on the test that is used [40]. In order to link inertial range anisotropy to the large-scale properties qualitatively and quantitatively, we need to distinguish first between different ''energy injection processes,'' which are specific to the large scales of each flow.

Specifically, one has to distinguish between nonhomogeneous scalar injection, as happens, e.g., when a large-scale temperature difference is applied across the system, resulting in a large-scale gradient, stationary [38] or decaying in time, and homogeneous scalar injection, as is the case for grid turbulence heated with a mandoline, the jets or the wakes on their axis. The former is known to lead to a large anisotropy, whereas the latter is essentially isotropic.

In fact, the equation developed in Ref. [28] was investigated for different mixings with the same injection characteristics: a mean temperature gradient applied on the large scales. It is not very surprising that a large-scale nonhomogeneity and anisotropy could influence the statistics up to relatively small scales. On the other hand, in a large-scale homogeneous and quasi-isotropic mixing, like a heated grid turbulence, one has to take properly into account the nonstationarity of the flow, in order to close the relation between different moments of temperature increment [41]. Our gen-

eral aim is, for finite Reynolds numbers (consequently when strict local isotropy generally does not hold), to understand how the large scales and the energy injection manner influence the inertial range evolution of different statistical quantities. In this paper, we investigate some of the mixings presented before, especially their isotropic properties, and analyze further the theory developed in Ref. [28], or its simpler form: Yaglom's equation. We consider mainly the problem of mixing by an homogeneous isotropic flow, with a nonhomogeneous scalar injection. This case is more complex than grid turbulence, but less complex than shear flows with a mean temperature gradient. DNS is a convenient way to produce such a flow configuration and to measure all the quantities [37] necessary to test our predictions. We study the statistical properties in a fixed plane Π perpendicular to $\vec{G}$, the scalar gradient, where $\vec{G}$ is parallel to the spatial direction z. In this plane Π ($z=\text{const}$), the isotropy of the scalar field has been shown numerically to be satisfied, by comparing the properties of the various moments of the temperature derivatives in the directions perpendicular to the gradient. This is in sharp contrast with the derivative parallel to the large-scale gradient [37].

To investigate how anisotropy is associated with the integral scales, we relax the 3D isotropy assumption and simply assume that the scalar is isotropic in the plane Π normal to the mean temperature gradient. In Sec. II, we first present some results concerning the theory based on the 3D isotropy assumption in order to provide data for comparison with results obtained using the 2D isotropy theory. We emphasize that for relatively small $\text{Pe}=\text{Re}\times\text{Pr}$ ($\text{Pr}=\nu/k_0$), the equation works well only for very small scales. In Sec. III, we present the hypotheses and the theoretical considerations that permit the derivation of a new evolution equation for the PDF's of passive scalar increments, which takes into account the mean temperature gradient. The closure needs five conditional averages. Some of them explicitly contain the large-scale anisotropy. In Sec. IV, we discuss the five conditional expectations obtained numerically. Finally, in Sec. V, we deduce a new Yaglom equation as a particular case of the PDF equation based on the 2D isotropy. The validity of this Yaglom equation is verified for various Pe numbers of the mixing and the balance between the terms is investigated. As shown in Sec. V, once the isotropy assumptions are adapted to a real situation, the PDF equation becomes a reliable tool for extrapolating small-scale PDF's from those obtained at large scales, and the original objective of Ref. [28] can be achieved.

II. PDF'S IN THE CONTEXT OF A THREE-DIMENSIONAL ISOTROPY

In this section, we present the numerical verification of the ''evolution'' equation for the PDF's of passive scalar increments derived in Ref. [28]. We demonstrate that this equation provides an accurate description of the PDF of scalar increments in a plane Π perpendicular to the mean gradient, and that the quantitative agreement becomes better when the scale becomes smaller and the Reynolds number becomes larger.

In the following, without loss of generality, we use a terminology referring to θ as the temperature. In this way, the ratio of the molecular diffusivity k_0 to the kinematic viscosity ν will be referred to as the Prandtl number Pr.

We now briefly present the strategy used to derive the PDF equation. The method is similar to that employed in Ref. [42] to obtain the PDF of the temperature itself. We will adopt the same procedure in this work (Sec. III), in order to obtain the PDF evolution equation through the scales when isotropy holds only in planes perpendicular to the mean gradient. The starting point is naturally the heat-transfer equation:

$$\frac{\partial\theta}{\partial t}(\vec{x},t)+\vec{u}\nabla\theta(\vec{x},t)=k_0\nabla^2\theta(\vec{x},t),$$

written in a point $\vec{x}$ at time t. We are then interested in temperature increments $X=\Delta\theta(\vec{x},\vec{r},t)$. The main steps of the mathematical development are the following.

(i) We consider a general test, scalar function $g(X,\vec{r})$. In particular, this function could be the nth-order (n even) temperature increment, $(\Delta\theta)^n$.

(ii) An operator $D_{[g]}$ is defined, which applies the operators involved in the heat-transfer equation to the function g:

$$D_{[g]}(\vec{x},\vec{r},t)\equiv\frac{\partial g(\Delta\theta(\vec{x},\vec{r},t),\vec{r})}{\partial t}+\vec{u}(\vec{x},t)\cdot\nabla g(\Delta\theta(\vec{x},\vec{r},t),\vec{r})$$
$$-k_0\nabla^2 g(\Delta\theta(\vec{x},\vec{r},t),\vec{r}).$$

(iii) When developed, the right-hand side can be simplified using the heat-transfer equation yielding a new equation. The statistical averages of both sides of the obtained equation are calculated using the following hypotheses: (i) stationarity of all statistical averages and (ii) three-dimensional homogeneity and isotropy. The latter can be expressed mathematically by the specific form of the operators gradient and Laplacian applied on the isotropic increment vector $\vec{r}$:

$$\nabla_{\vec{r}}\equiv\frac{1}{r^2}\frac{\partial}{\partial r}r^2,$$

where $r=|\vec{r}|$. These hypotheses and the corresponding algebraic manipulations are very similar in spirit to the one used in Ref. [31]. The final form of these developments is the functional equation $\langle\mathcal{F}(g)\rangle=0$, where $\mathcal{F}$ is the functional of g,

$$\int g\mathcal{E}(P(r,X))dX=0,\quad\forall g,\tag{1}$$

equivalent, in the distributive sense, to the equation

$$\mathcal{E}(P(r,X))=0,$$

considered as the partial differential equation for the probability density function P, depending on the modulus r of the spatial displacement and the stochastic variable X representing the temperature increment $\Delta\theta$. Let us note that the same approach was used in Ref. [42]. The resulting equation then reads, explicitly,

$$\left[\frac{2}{r}+\frac{\partial}{\partial r}\right][P(r,X)q_1(r,X)]+2k_0\frac{\partial^2}{\partial X^2}[P(r,X)q_2(r,X)]$$
$$=2k_0\left[\frac{2}{r}+\frac{\partial}{\partial r}\right]\frac{\partial P}{\partial r}(r,X), \quad (2)$$

where $P(r,X)$, $q_1(r,X)$, and $q_2(r,X)$ are the PDF of temperature increment, the conditional expectation of the velocity increment, and the squared temperature gradient conditioned by the temperature increment, respectively. It is convenient to use a dimensionless version of Eq.(2), by using the rescaled variables: $\tilde{r}=r/\lambda_\theta$, $\tilde{u}=u/u'$, and $\tilde{X}=X/\theta'$ where $\lambda_\theta\equiv\theta'/\langle(\partial\theta/\partial x)^2\rangle^{1/2}$ is the temperature Taylor scale (also called Oboukhov-Corrsin microscale); θ' is the temperature rms. Thereafter we drop the tilde:

$$\frac{\mathrm{Pe}}{2}\left[\frac{2}{r}+\frac{\partial}{\partial r}\right][P(r,X)q_1(r,X)]+\frac{\partial^2}{\partial X^2}[P(r,X)q_2(r,X)]$$
$$=\left[\frac{2}{r}+\frac{\partial}{\partial r}\right]\frac{\partial P}{\partial r}(r,X). \quad (3)$$

Equation (3) is then written symbolically as I+II=III, the three terms I, II, and III referring to the three terms as they appear in Eq. (3).

The well-known Yaglom equation can be simply obtained from 1 by choosing $g=(\Delta\theta)^2$, and by integrating once with respect to r. Yaglom's equation [30] simply reads

$$-\langle(\Delta u)(\Delta\theta)^2\rangle+2k_0\frac{d}{dr}\langle(\Delta\theta)^2\rangle=\frac{4}{3}\overline{N}r, \quad (4)$$

where $\overline{N}=k_0\langle(\nabla\theta)^2\rangle$. Equation (4) is written for simplicity as $A+B=C$.

The three terms I, II, and III have the same origin in the heat equation, and the same physical interpretation as the three terms *A*, *C*, and *B* (in this order). Yaglom's equation represents an energy balance. Terms I and *A* come from the advection term in the heat transport equation; they represent the energy transfer through the scales by the turbulent process.

Term II comes from a part of the molecular diffusion, and it represents a large-scale diffusion. Term *C*, its counterpart, is the mean energy transfer rate between the scales. Finally, terms III and *B* both are the expression of the molecular diffusion, and they are present at small scales only.

Since the equation has been derived using the assumptions of homogeneity and three-dimensional isotropy, the PDF $P(r,X)$ and the conditional expectation of the squared temperature gradient $q_2(r,X)=\langle(\nabla\theta)^2/\Delta\theta\rangle$ depend on $r=|\vec{r}|$ only. In addition, since the conditional expectation of the velocity increment is isotropic, $\langle\Delta\vec{u}/\Delta\theta\rangle=q_1(r,X)\vec{r}/r$, and $q_1(r,X)$ is thus easily amenable to measurements as it is the conditional expectation of the longitudinal velocity increment. The closure problem then consists in determining the two scalar functions $q_1(r,X)$ and $q_2(r,X)$.

The conditional expectations $q_1(r,X)$ and $q_2(r,X)$ were previously determined in two cases: from our measurements in a boundary layer over a heated wall [29], and from DNS of a passive scalar with a mean gradient mixed by a homogeneous and isotropic turbulent velocity field [37,33]. Isotropy implies that all the quantities involved in Eq. (3) are even functions of X: $P(r,X)=P(r,-X)$, $q_1(r,X)=q_1(r,-X)$, and $q_2(r,X)=q_2(r,-X)$. If the mixing is not isotropic, these constraints do not hold.

The experimental conditional expectations were therefore symmetrized to provide closure functions consistent with the isotropic theory [33]. Still, the parity of the functions does not guarantee isotropy, so the results we obtain for the analysis of this equation remain, in spite of this symmetrization, very sensitive to the isotropy of the experimental or DNS data.

To provide a basis for comparison with our following proposed 2D isotropy theory, we now present results of the 3D equation, showing to what extent Eq. (3) is verified for Reynolds numbers $R_\lambda=40$ and 70 and Prandtl numbers $\mathrm{Pr}=0.5$ or $\mathrm{Pr}=1$ keeping a fixed mean temperature gradient $G=1$. All the quantities are made dimensionless with respect to the computational domain size. In order to determine the velocity and temperature fields numerically, the Navier-Stokes and heat-transport equations are solved using a standard pseudospectral code. The boundary conditions for velocity and temperature are periodic in the three directions. The computational domain is periodic with a length 2π, containing 128^3 points. A good statistical convergence could be achieved by averaging for about six eddy-turnover times. In our calculations, we have checked that the moments of the scalar derivatives in directions perpendicular to the gradient do not depend, up to statistical errors, on the precise direction in the plane parallel. More details about the numerical method used in this work can be found in Ref. [37]. Let us consider a first case with the following parameters:

(i) $R_\lambda=40$, $\mathrm{Pr}=1$, $G=1$. The characteristics of the mixing are $k_0=\nu=0.012$, the rms of temperature fluctuations $\theta'=1.79$, the Oboukhov-Corrsin microscale $\lambda_\theta=0.235$, and the Kolmogorov scale of the turbulent dynamic field $\eta=0.057$. The nondimensionalized (not symmetrized) conditional expectations $\tilde{q}_1=\mathrm{Pe}_{\lambda_\theta}/2\langle\Delta u/\Delta\theta\rangle$ and $\tilde{q}_2=\lambda_\theta^2\langle(\nabla\theta)^2/\Delta\theta\rangle$, obtained from DNS data, are presented in Fig. 1. For simplicity, we will further note $\tilde{q}_1$ and $\tilde{q}_2$ as q_1 and q_2. All the conditional expectations, terms in Eq. (3) or (4) analyzed thereafter are dimensionless.

The PDF's obtained from DNS data in the plane perpendicular to the mean gradient are presented in Fig. 2. The figure reflects well the evolution from a large-scale Gaussian to a small-scale PDF with typical exponential tails.

Using these PDF's and conditional expectations, we verify Eq. (3), by simply computing the three terms. As stated in Ref. [33] (see Fig. 2 of Ref. [33]) the residual of the equation is maximal at $X=0$, so we present the equation verification at $X=0$ only. Although a nondimensionalization using the Oboukhov-Corrsin microscale λ_θ appears to be more convenient for the numerical treatment of the equation [33], the results are represented in terms of r/η. Figure 3 shows that the equation is verified only for $r\leqslant 7\eta$ indicating the lack of isotropy at larger scales. The reason for this is the large discrepancy between the ''turbulent transport'' term I that tends rapidly to zero at large scales, and the ''diffusion'' term II that remains almost constant for large scales. These

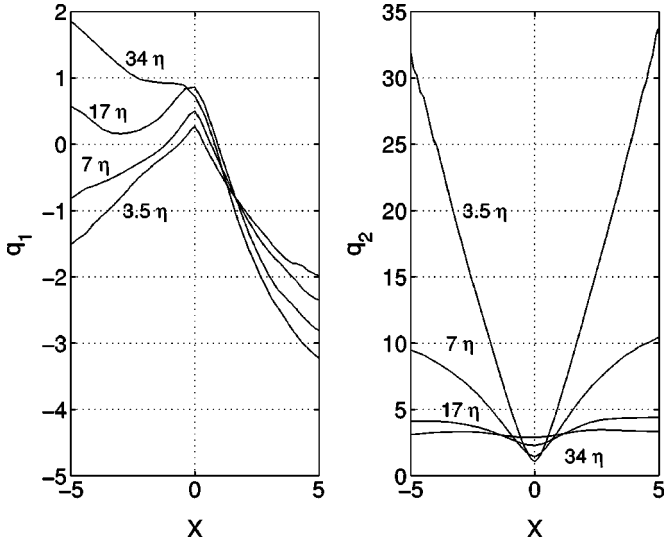

FIG. 1. Conditional expectations q_1 (left) and q_2 (right), for the scales 3.5η, 7η, 17η, and 34η, at $R_\lambda=40$ and Pr=1.

features are not surprising since they are obviously associated with the widely documented behavior of Yaglom's equation [43]. As Fig. 10 will illustrate it, the term $C=\frac{4}{3}\overline{Nr}$ which is associated with the term II of Eq. (3), remains unbalanced at large scales, when the turbulent transport term $A=-\langle\Delta u(\Delta\theta)^2\rangle$ becomes small. Note that this term A was modeled in Ref. [20] in terms of an eddy diffusivity characteristic of the dispersive properties of the velocity field alone, *à la Richardson*.

All the above quantities have been computed in the plane normal to the mean gradient. In experiments, e.g., in a heated boundary layer, this should correspond to data obtained by treating the cold wire measurements using Taylor's hypothesis. Using the same DNS data we can also check what happens in the direction parallel to the mean gradient. It appears that, in this case, Eq. (3) does not hold even for the smallest scales. Anisotropy affects even the dissipative scales in this direction, as already emphasized in Ref. [37]. In Fig. 4 we

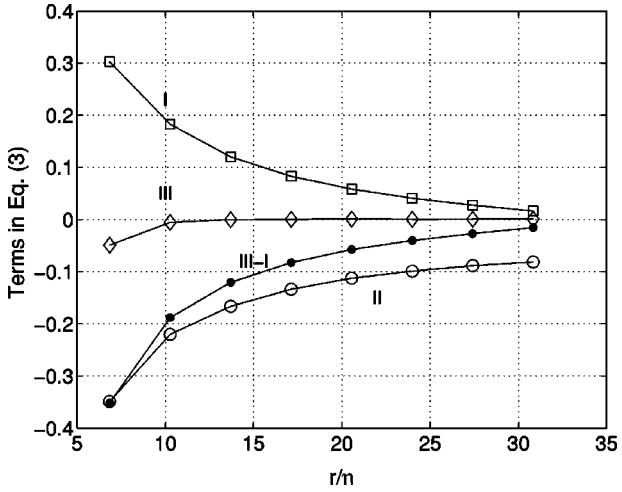

FIG. 3. $X=0$ evolution for the three terms in Eq. (3), at $R_\lambda=40$ and Pr=1. The term II (○) is to be compared to III−I (●).

present the computed conditional expectations, and in Fig. 5 the PDF's obtained by treating the DNS data in the direction parallel to the mean gradient $\vec{G}$.

One can notice the strong asymmetry of the represented quantities indicative of the strong anisotropy in this direction. The trend of the two conditional expectations and the PDF's to become symmetric at the smallest scale (3.5η) is, nevertheless, clear. This behavior demonstrates the anisotropy in the mean temperature gradient direction, and motivates the investigation of the mixing when isotropy holds in planes only.

The effect of the Prandtl number has been investigated by comparing the first case above (Figs. 1–3) to that with Pr =0.5. The conditional expectations q_1 and q_2 are presented in Fig. 6, and the PDF's in Fig. 7.

Though the conditional expectations q_1 and q_2 are more symmetric for a smaller Prandtl number, Eq. (3) is even less verified in this case. This is associated with the fact that the Péclet number Pe is smaller, so that the imbalance of Eq. (3) for large scales is stronger (see Fig. 8).

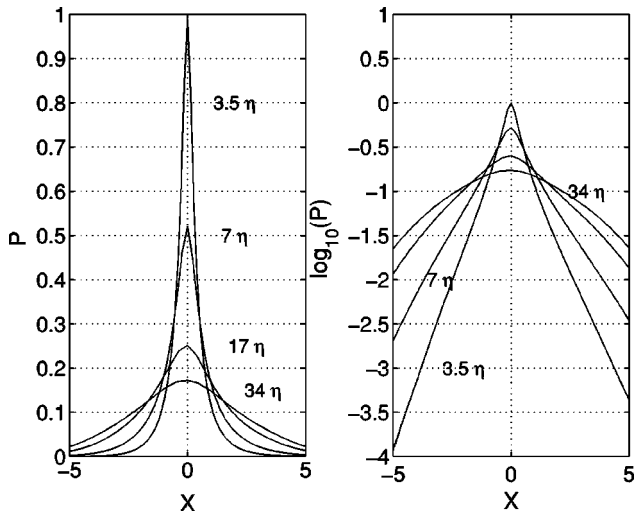

FIG. 2. PDF's in the plane perpendicular to the mean gradient for the scales 3.5η, 7η, 17η, and 34η, using a linear scale (left) and a logarithmic scale (right), at $R_\lambda=40$ and Pr=1.

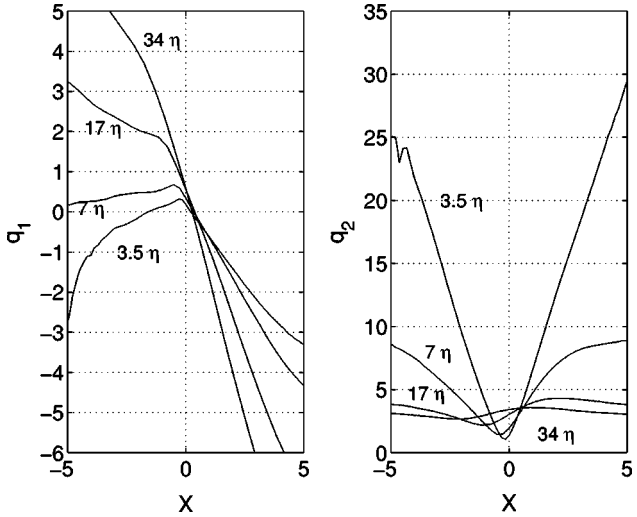

FIG. 4. Conditional expectations q_1 and q_2 for the scales 3.5η, 7η, 17η, and 34η, in the direction parallel to the mean gradient, at $R_\lambda=40$ and Pr=1.

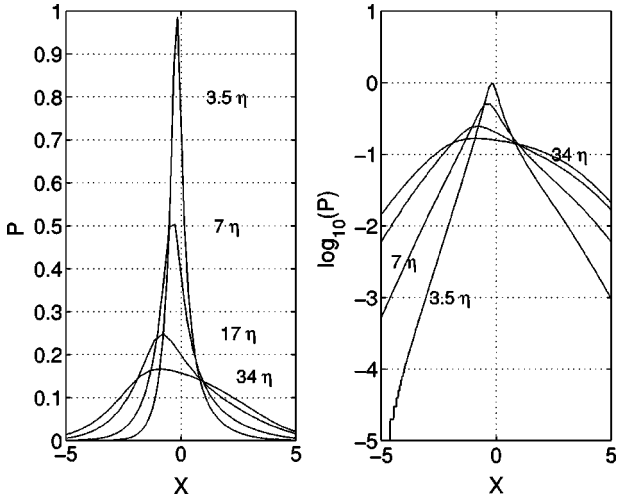

FIG. 5. PDF's for the scales 3.5η, 7η, 17η, and 34η, in the direction parallel to the mean gradient, at $R_\lambda = 40$ and Pr=1.

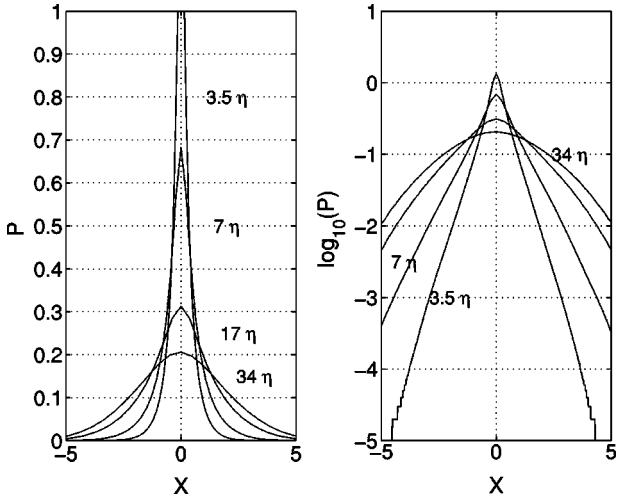

FIG. 7. PDF's for the scales 3.5η, 7η, 17η, and 34η, at $R_\lambda = 40$ and Pr=0.5.

In contrast, a higher Reynolds number modifies the velocity field by extending the inertial zone so that isotropy then appears to be verified for larger scales in terms of the Kolmogorov length scale. Another way to write Eq. (3) is (III−I)/II=1. Thus, comparing the term (III−I)/II with the value 1 is a compact way to emphasize the validation domain for the equation as a function of the Péclet number of the mixing. Figure 9 represents such a result, for $X=0$: the larger the Péclet number is, the better the equation is verified. We note that, for Pe=82, the approach becomes better for the scales smaller that 30η, with an error of about 20%.

In this sense, the direct influence of the large scale anisotropy diminishes as one reaches smaller and smaller scales. Equivalently, the range of scales where the equation is valid increases when the Péclet number increases.

As already mentioned, Yaglom's equation (4) is obtained as a particular case of the approach; moreover, it is easier to verify the second-order relation between the moments. Equation (4), rendered dimensionless using the same quantities as for Eq. (3), is analyzed through the data reported in Fig. 10.

We can note that the disagreement with the full isotropy predictions in terms of Yaglom's equation is very similar to that for Eq. (3) taken at $X=0$. (See Fig. 3.) The conclusion is that Yaglom's equation is a good indicator of the validity domain for Eq. (3), being obviously less complete, but simpler than the equation for the PDF's. Yaglom's equation does not contain any intermittency effect, but it is a useful means to investigate isotropy.

The general conclusion of this section is that, for finite Reynolds numbers, the equation which assumes 3D isotropy allows us to determine quantitatively the PDF shapes in the plane perpendicular to the mean gradient, but only at small scales and large Péclet number. Important deviations are found at larger scales, in the upper part of the inertial range. In order to investigate the laws governing the evolutions for the large inertial scales, in Sec. III we develop an approach which assumes small-scale isotropy only in planes perpendicular to the mean gradient.

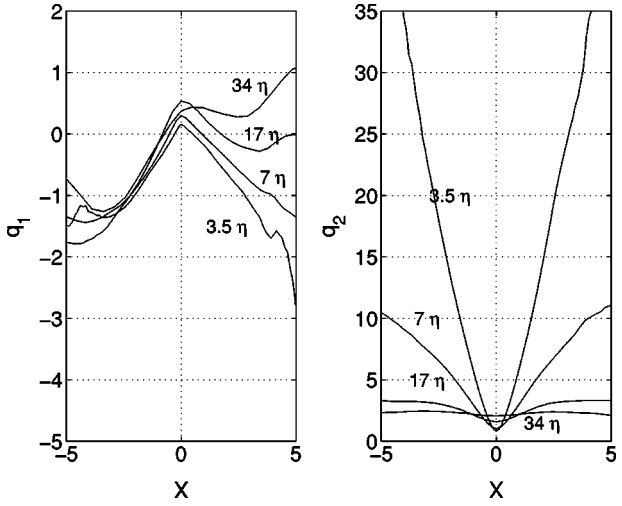

FIG. 6. Conditional expectations q_1 and q_2 for the scales 3.5η, 7η, 17η, and 34η, at $R_\lambda = 40$ and Pr=0.5.

III. CONSEQUENCES OF ISOTROPY RESTRICTED TO A PLANE

Section II (see also Ref. [33]) demonstrated that the isotropy assumption for the mixing of a passive scalar with a

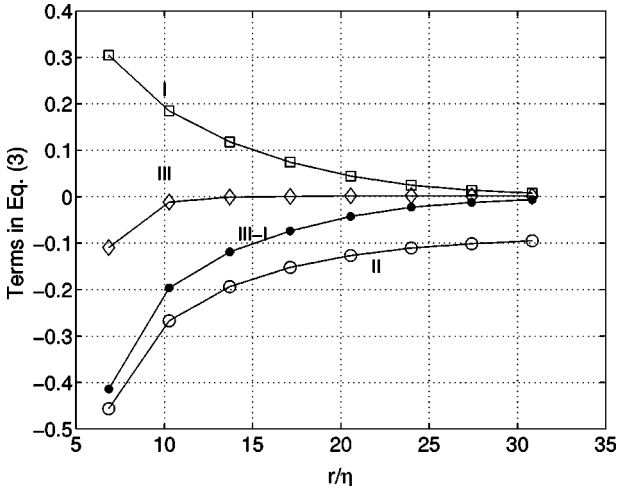

FIG. 8. $X=0$ evolution for the three terms involved in Eq. (3), at $R_\lambda = 40$ and Pr=0.5. The term II (○) is to be compared to III−I (●).

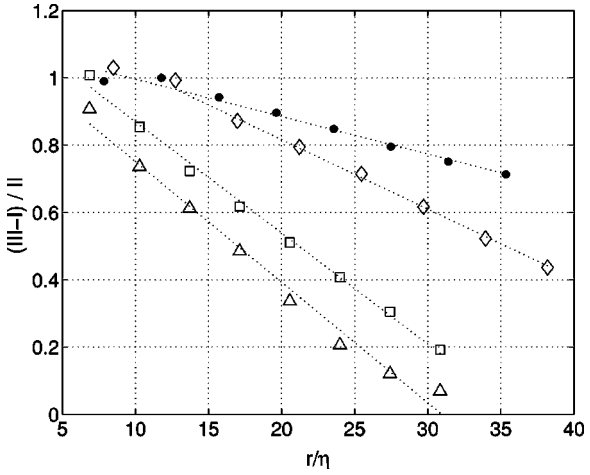

FIG. 9. $X=0$ evolution for the ratio (III−I)/II in Eq. (3), which should be compared with the value 1, function of the scales r/η, for different Péclet numbers: Pe=20 (△), Pe=40 (□), Pe=70 (◇), and Pe=82 (●).

mean gradient leads to a good balance between the terms in the equation describing the evolution of the PDF's of scalar increments in a plane perpendicular to the mean gradient, at small scales and at large Péclet numbers. Our approach, however, does work at all for scalar differences parallel to the mean gradient. This shows the limitations of the 3D isotropy assumption for the problem studied, and suggests, instead, a weaker isotropy assumption considered only in a plane perpendicular to the mean gradient, or, in general, perpendicular to the anisotropy direction. The purpose of this section is the derivation of the equation of evolution for the PDF's, assuming isotropy only in planes perpendicular to $\vec{G}$.

A. Theory

In the following derivation, we propose a more general form of the evolution equation of the PDF. It is a generalization of the demonstration proposed in Ref. [28] and rapidly presented in Sec. II. Let $g(X,\vec{r})$ be a scalar function of a scalar variable X and a vector $\vec{r}$. We assume that $g \in \mathcal{S}(R^4)$, $\mathcal{S}$ being the space of infinitely differentiable rapidly decreasing functions.

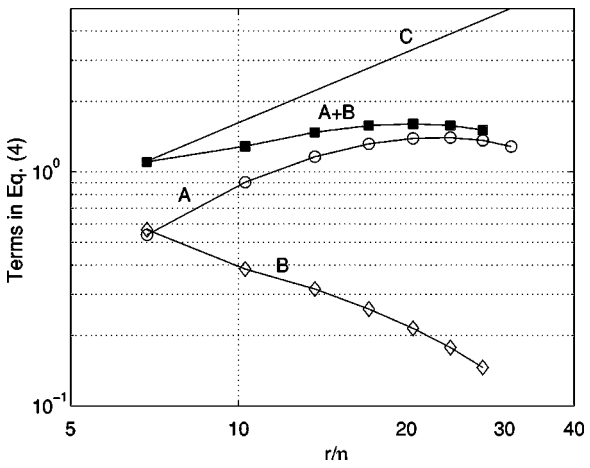

FIG. 10. Yaglom's equation nonverification, for $R_\lambda=40$ and Pr=1. $A+B$ (■) is to be compared with C (continuous line).

The variable X describes the value of increments $X=\Delta\theta(\vec{x},\vec{r},t)=\theta(\vec{x}+\vec{r},t)-\theta(\vec{x},t)$, where $\vec{r}$ is the separation vector. We define

$$D[g](\vec{x},\vec{r},t)\equiv\frac{\partial g(\Delta\theta(\vec{x},\vec{r},t),\vec{r})}{\partial t}+\vec{u}(\vec{x},t)\cdot\nabla_{\vec{x}}g(\Delta\theta(\vec{x},\vec{r},t),\vec{r})$$
$$-k_0\nabla^2_{\vec{x}}g(\Delta\theta(\vec{x},\vec{r},t),\vec{r}). \quad (5)$$

Using the equation of evolution for a passive scalar,

$$\frac{\partial\theta}{\partial t}(\vec{x},t)+\vec{u}(\vec{x},t)\cdot\nabla_{\vec{x}}\theta(\vec{x},t)-k_0\nabla^2_{\vec{x}}\theta(\vec{x},t)=0, \quad (6)$$

and elementary algebraic manipulations, one finds

$$D[g](\vec{x},\vec{r},t)=-\frac{\partial g}{\partial X}(\Delta\theta(\vec{x},\vec{r},t),\vec{r})\Delta\vec{u}(\vec{x},\vec{r},t)\cdot\nabla_{\vec{x}}\theta(\vec{x}+\vec{r},t)$$
$$-k_0\frac{\partial^2 g}{\partial X^2}(\Delta\theta(\vec{x},\vec{r},t),\vec{r})[\nabla_{\vec{x}}\Delta\theta(\vec{x},\vec{r},t)]^2, \quad (7)$$

where $\Delta\vec{u}(\vec{x},\vec{r},t)=\vec{u}(\vec{x}+\vec{r},t)-\vec{u}(\vec{x},t)$.

We consider statistically stationary flows, and we assume that the flow properties are homogeneous in planes $\Pi,z=cst$. This is *a priori* compatible with a mean velocity profile $\vec{U}=(U_x(z),U_y(z),U_z(z))$. We found, however, that in the simplest possible shear flow, $\vec{U}=(Sz,0,0)$, the isotropy of the scalar in $z=cst$ planes was not a good approximation at all, and we restrict ourselves here to the case where the mean velocity profile is uniform, and the flow is homogeneous and isotropic. In the following, we will simply compute the statistical averages over the plane $\Pi,z=cst$:

$$\langle\varphi\rangle(z)\equiv\lim_{R\to\infty}\frac{1}{\pi R^2}\int_{(x^2+y^2)<R^2}\varphi(\vec{x})dx\,dy. \quad (8)$$

Note that the average of a gradient, in the sense of Eq. (8) is non-zero: $\langle\nabla\vec{f}\rangle(z)=\langle\partial_z f_z\rangle$. The mean values of quantities such as $D[g]$ are functions of z and of the separation vector $\vec{r}$.

Specifically, the mean value of expression (5) reads

$$\langle D[g]\rangle(\vec{r},z)=\partial_z\langle u_z(\vec{x},t)g(\Delta\theta(\vec{x},\vec{r},t),\vec{r})\rangle(\vec{r},z)$$
$$-k_0\partial_z^2\langle g(\Delta\theta(\vec{x},\vec{r},t),\vec{r})\rangle(\vec{r},z). \quad (9)$$

A large-scale anisotropy, such as that encountered in the proximity of the solid wall in a turbulent boundary layer, is likely to induce a strong anisotropy of all the investigated structures. A symmetry between increments may be expected only in a plane perpendicular to the direction of anisotropy. For this reason, we restrict ourselves in the following to separation vectors $\vec{r}$ in the plane Π normal to $\vec{z}$: $\vec{r}\cdot\vec{z}=0$.

Keeping in mind that the averages [Eq. (8)] are taken only in the (x,y) plane, and exchanging the order of z derivatives and averaging integrals, we can rewrite the right-hand side of Eq. (9) in the following form:

$$\langle D[g]\rangle(\vec{r},z)=\left\langle u_z(\vec{x},t)\frac{\partial g}{\partial X}(\Delta\theta(\vec{x},\vec{r},t),\vec{r})\partial_z\Delta\theta(\vec{x},\vec{r},t)\right\rangle(\vec{r},z)+\langle\partial_z u_z(\vec{x},t)g(\Delta\theta(\vec{x},\vec{r},t),\vec{r})\rangle(\vec{r},z)$$
$$-k_0\left\langle\frac{\partial^2 g}{\partial X^2}(\Delta\theta(\vec{x},\vec{r},t),\vec{r})[\partial_z\Delta\theta(\vec{x},\vec{r},t)]^2\right\rangle(\vec{r},z)-k_0\left\langle\frac{\partial g}{\partial X}(\Delta\theta(\vec{x},\vec{r},t),\vec{r})\partial_z^2\Delta\theta(\vec{x},\vec{r},t)\right\rangle(\vec{r},z). \quad (10)$$

On the other hand, taking the average of Eq. (7), we obtain

$$\left\langle\frac{\partial g}{\partial X}(\Delta\theta(\vec{x},\vec{r},t),\vec{r})\Delta\vec{u}(\vec{x},\vec{r},t)\cdot\nabla_{\vec{x}}\theta(\vec{x}+\vec{r},t)\right\rangle(\vec{r},z)+k_0\left\langle\frac{\partial^2 g}{\partial X^2}(\Delta\theta(\vec{x},\vec{r},t),\vec{r})[\nabla_{\vec{x}}\Delta\theta(\vec{x},\vec{r},t)]^2\right\rangle(\vec{r},z)+\langle D[g]\rangle(\vec{r},z)=0. \quad (11)$$

Combining Eqs. (10) and (11), we obtain an equation whose terms can be further transformed following a general strategy which consists in eliminating, wherever possible, the derivatives of temperature increments with respect to x and y. Specifically, to transform the first term on the right-hand side of Eq. (11), we use the obvious equality

$$\frac{\partial\theta}{\partial x_i}(\vec{x}+\vec{r},t)=\frac{\partial\theta}{\partial r_i}(\vec{x}+\vec{r},t),\quad i=1,2, \quad (12)$$

and the continuity equation for $\vec{u}$:

$$\left\langle\frac{\partial g}{\partial X}(\Delta\theta(\vec{x},\vec{r},t),\vec{r})\Delta\vec{u}(\vec{x},\vec{r},t)\cdot\nabla_{\vec{x}}\theta(\vec{x}+\vec{r},t)\right\rangle(\vec{r},z)$$
$$=\nabla_{\vec{r}}\langle g(\Delta\theta(\vec{x},\vec{r},t),\vec{r})\Delta\vec{u}(\vec{x},\vec{r},t)\rangle(\vec{r},z)-\langle[\nabla_{\vec{r}}g](\Delta\theta(\vec{x},\vec{r},t),\vec{r})\Delta\vec{u}(\vec{x},\vec{r},t)\rangle(\vec{r},z)$$
$$+\langle\partial_z u_z(\vec{x}+\vec{r},t)g(\Delta\theta(\vec{x},\vec{r},t),\vec{r})\rangle(\vec{r},z)+\left\langle\frac{\partial g}{\partial X}(\Delta\theta(\vec{x},\vec{r},t),\vec{r})\Delta u_z(\vec{x},\vec{r},t)\partial_z\theta(\vec{x}+\vec{r},t)\right\rangle(\vec{r},z). \quad (13)$$

We proceed similarly for the other terms (see the Appendix for details) to arrive at

$$\left\langle\frac{\partial g}{\partial X}(\Delta\theta(\vec{x},\vec{r},t),\vec{r})\cdot\Delta[u_z\partial_z\theta](\vec{x},\vec{r},t)\right\rangle+\nabla_{\vec{r}}\langle g(\Delta\theta(\vec{x},\vec{r},t),\vec{r})\Delta\vec{u}(\vec{x},\vec{r},t)\rangle(\vec{r},z)-\langle[\nabla_{\vec{r}}g](\Delta\theta(\vec{x},\vec{r},t),\vec{r})\Delta\vec{u}(\vec{x},\vec{r},t)\rangle(\vec{r},z)$$
$$+k_0\left\{\left\langle\left[\frac{\partial^2 g}{\partial X^2}(-\Delta\theta(\vec{x},-\vec{r},t),\vec{r})+\frac{\partial^2 g}{\partial X^2}(\Delta\theta(\vec{x},\vec{r},t),\vec{r})\right](\nabla_{(x,y)}\theta(\vec{x},t))^2\right\rangle(\vec{r},z)-2\langle\nabla_{\vec{r}}^2 g(\Delta\theta(\vec{x},\vec{r},t),\vec{r})\rangle(\vec{r},z)\right.$$
$$\left.-\left\langle\frac{\partial g}{\partial X}(\Delta\theta(\vec{x},\vec{r},t),\vec{r})\partial_z^2\Delta\theta(\vec{x},\vec{r},t)\right\rangle(\vec{r},z)-2\nabla_{\vec{r}}\left\langle\left[\frac{\partial g}{\partial X}(\Delta\theta(\vec{x},\vec{r},t),\vec{r})\nabla_{(x,y)}\theta(\vec{x},t)-\nabla_{\vec{r}}g(\Delta\theta(\vec{x},\vec{r},t),\vec{r})\right]\right\rangle(\vec{r},z)\right\}$$
$$+\langle g(X,\vec{r})\partial_z u_z(\vec{x}+\vec{r},t)\rangle(\vec{r},z)+\langle g(X,\vec{r})\partial_z u_z(\vec{x},t)\rangle(\vec{r},z)=0. \quad (14)$$

By $\Delta[u_z\partial_z\theta](\vec{x},\vec{r},t)$ we mean the increment of the function inside the brackets, i.e., $\Delta[u_z\partial_z\theta](\vec{x},\vec{r},t)\equiv u_z(\vec{x}+\vec{r},t)\partial_z\theta(\vec{x}+\vec{r},t)-u_z(\vec{x},t)\partial_z\theta(\vec{x},t)$. The resulting equation (14) can now be integrated over the $\vec{r}$ variable in R^2. The free choice of $g\in\mathcal{S}$ makes it possible to select values corresponding to a restricted neighborhood of a given vector $\vec{r}$ and, in the limit of g approaching a Dirac distribution, to describe a sharp value of $\vec{r}$ provided the corresponding mean values exist in the sense of distributions. Integrating Eq. (14) over the whole $\vec{r}$ space will make the divergence terms disappear. Let us denote the $\vec{r}$ integrals by $\langle.\rangle$: $\langle\varphi\rangle\equiv\int_{R^2}\varphi(\vec{r})d^2r$. Equation (14) thus yields

$$\left\langle\left\langle\frac{\partial g}{\partial X}(X,\vec{r})\cdot\Delta[u_z\partial_z\theta](\vec{x},\vec{r},t)\right\rangle\right\rangle(z)$$
$$-\langle\langle[\nabla_{\vec{r}}g](\Delta\theta(\vec{x},t),\vec{r})\Delta\vec{u}(\vec{x},t)\rangle\rangle(z)+k_0\left\{\left\langle\left\langle\left[\frac{\partial^2 g}{\partial X^2}(-\Delta\theta(\vec{x},-\vec{r},t),\vec{r})+\frac{\partial^2 g}{\partial X^2}(\Delta\theta(\vec{x},t),\vec{r})\right](\nabla_{(x,y)}\theta(\vec{x},t))^2\right\rangle\right\rangle(z)\right.$$
$$\left.-2\langle\langle\nabla_{\vec{r}}^2 g(\Delta\theta(\vec{x},t),\vec{r})\rangle\rangle(z)-\left\langle\left\langle\frac{\partial g}{\partial X}(\Delta\theta(\vec{x},t),\vec{r})\partial_z^2\Delta\theta(\vec{x},t)\right\rangle\right\rangle(z)\right\}+\langle\langle g(X,\vec{r})\partial_z[u_z(\vec{x},t)+u_z(\vec{x}+\vec{r},t)]\rangle\rangle(z)=0. \quad (15)$$

B. Evolution equation for the PDF

Let us introduce the stochastic variables:

$$X=\Delta\theta(\vec{x},\vec{r},t),\quad \vec{Y}\equiv(Y_x,Y_y)=(\Delta u_x(\vec{x},\vec{r},t),\Delta u_y(\vec{x},\vec{r},t)),\quad Z=[\nabla_{(x,y)}\theta(\vec{x},t)]^2,$$

$$S=\partial_z^2\Delta\theta(\vec{x},\vec{r},t),\quad T=\partial_z u_z(\vec{x}+\vec{r},t)+\partial_z u_z(\vec{x},t),\quad W=\Delta\left[u_z\frac{\partial\theta}{\partial z}\right], \tag{16}$$

and the corresponding PDF

$$\tilde{P}(\vec{r},z,X,\vec{Y},Z,S,T,W)=P(\vec{r},z,X)Q(\vec{r},z,\vec{Y},Z,S,T,W/X), \tag{17}$$

where $Q(\vec{r},z,\vec{Y},Z,S,T,W/X)$ denotes a conditional probability. By replacing the spatial (x,y) averages with ensemble averages, we can rewrite the mean values $\langle\langle\cdot\rangle\rangle$ as follows:

$$\langle\langle\cdot\rangle\rangle(z)=\int\tilde{P}(\vec{r},z,X,\vec{Y},Z,S,T,W)d^2r\,dX\,d^2Y\,dZ\,dS\,dT\,dW.$$

As a result, Eq. (15) now reads

$$\begin{aligned}&\int\frac{\partial g}{\partial X}(X,\vec{r})q_3(\vec{r},z,X)P(\vec{r},z,X)d^2r\,dX-\int[\nabla_{\vec{r}}g](X,\vec{r})\vec{q}_1(\vec{r},z,X)P(\vec{r},z,X)d^2r\,dX\\&+k_0\Bigg\{\int\frac{\partial^2 g}{\partial X^2}(X,\vec{r})[q_2(-\vec{r},z,-X)P(-\vec{r},z,-X)+q_2(\vec{r},z,X)P(\vec{r},z,X)]d^2r\,dX\\&-2\int\nabla_{\vec{r}}^2 g(X,\vec{r})P(\vec{r},z,X)d^2r\,dX-\int\frac{\partial g}{\partial X}(X,\vec{r})q_4(\vec{r},z,X)P(\vec{r},z,X)d^2r\,dX\Bigg\}\\&+\int g(X,\vec{r})q_5(\vec{r},z,X)P(\vec{r},z,X)d^2r\,dX=0,\end{aligned} \tag{18}$$

where we have introduced the conditional expectations on the scalar increments:

$$\vec{q}_1(\vec{r},z,X)=\langle\Delta\vec{u}/\Delta\theta\rangle, \tag{19}$$

$$q_2(\vec{r},z,X)=\langle(\nabla\theta)^2_{xy}/\Delta\theta\rangle=\langle[(\nabla_x\theta)^2+(\nabla_y\theta)^2]/\Delta\theta\rangle, \tag{20}$$

$$q_3(\vec{r},z,X)=\left\langle\Delta\left[u_z\frac{\partial\theta}{\partial z}\right]\Big/\ \Delta\theta\right\rangle, \tag{21}$$

$$q_4(\vec{r},z,X)=\langle\partial_z^2\Delta\theta/\Delta\theta\rangle, \tag{22}$$

$$q_5(\vec{r},z,X)=\langle 2\partial_z u_z+\Delta\partial_z u_z/\Delta\theta\rangle. \tag{23}$$

The conditional average $\vec{q}_1$ is simply defined by

$$\vec{q}_1(\vec{r},z,X)=\frac{1}{P(\vec{r},z,X)}\int\vec{Y}\tilde{P}(\vec{r},z,X,\vec{Y},Z,S,T,W)d^2Y\,dZ\,dS\,dT\,dW,$$

and similar definitions are used for the other quantities.

Since g is an arbitrary test function from $\mathcal{S}(R^4)$, Eq. (18) is a weak form of

$$\begin{aligned}&-\frac{\partial}{\partial X}(\tilde{q}_3(\vec{r},z,X)P(\vec{r},z,X))+\nabla_{\vec{r}}[\vec{q}_1(\vec{r},z,X)P(\vec{r},z,X)]\\&+2k_0\frac{\partial^2}{\partial X^2}[\tilde{q}_2(\vec{r},z,X)P(\vec{r},z,X)]-2k_0\nabla_{\vec{r}}^2P(\vec{r},z,X)+q_5(\vec{r},z,X)P(\vec{r},z,X)=0,\end{aligned} \tag{24}$$

where

$$\tilde{q}_2(\vec{r},z,X) \equiv \tfrac{1}{2}[q_2(-\vec{r},z,-X)+q_2(\vec{r},z,X)] \qquad (25)$$

and

$$\tilde{q}_3(\vec{r},z,X) \equiv k_0 q_4(\vec{r},z,X) - q_3(\vec{r},z,X). \qquad (26)$$

In this form, it is clear that only four independent closure functions arise in Eq. (24). So far, we have used in the derivation of Eq. (24) *only* the assumption of homogeneity in the (x,y) plane. In Sec. III C we shall investigate the consequences of the 2D isotropy assumption.

It is easily seen from the definitions (16) that the probability density function $\tilde{P}(\vec{r},z,X,\vec{Y},Z,S,T)$ possesses the following symmetry property with respect to the reflection of $\vec{r}$:

$$\tilde{P}(\vec{r},z,X,\vec{Y},Z,S,T) = \tilde{P}(-\vec{r},z,-X,-\vec{Y},Z,-S,T). \quad (27)$$

The probability density function $P(\vec{r},z,X)$ thus satisfies $P(\vec{r},z,X)=P(-\vec{r},z,-X)$, and

$$\vec{q}_1(\vec{r},z,X) = -\vec{q}_1(-\vec{r},z,-X),$$

$$q_i(\vec{r},z,X) = q_i(-\vec{r},z,-X), \quad i=2,5,$$

$$q_i(\vec{r},z,X) = -q_i(-\vec{r},z,-X), \quad i=3,4. \qquad (28)$$

As a result, $\tilde{q}_2$ in Eq. (25) is simply equal to q_2.

C. Local isotropy

For an arbitrary scalar field φ and an arbitrary vector field $\vec{v}$ depending on the space variables $\vec{r}$, the local isotropy condition in the (x,y) plane can be expressed as follows.

2D Assumption. $\langle\varphi\rangle(\vec{r},z)=\langle\varphi\rangle(r,z)$, $(r = |\vec{r}|)$, and $\langle v_i\rangle(\vec{r},z)=w(r,z)(r_i/r)$ $(i=1$, and 2). The scalar function $w(r,z)$ is obviously equal to $[\langle v_i\rangle\langle v_i\rangle]^{1/2}$ or, equivalently, to $\langle v_i\rangle r_i/r$. We shall denote $\langle v_i\rangle(r_i/r)\equiv\langle v_L\rangle$, and write $\langle v_i\rangle(\vec{r})=\langle v_L\rangle(r)(r_i/r)$. The stochastic variables X, Z, S, W, and T are scalars from the point of view of the 2D geometry in the (x,y) plane. Under the 2D assumption, the scalar functions $P(\vec{r},z,X)$, $q_2(\vec{r},z,X)$, $q_3(\vec{r},z,x)$, $q_4(\vec{r},z,X)$, and $q_5(\vec{r},z,X)$ are functions of r only. The Laplace operator thus simplifies to $\nabla_{\vec{r}}^2 = r^{-1}(\partial/\partial r)[r(\partial/\partial r)]$. As far as the vector $\vec{q}_1(\vec{r},z,X)$ is concerned, the isotropy assumption yields: $\vec{q}_1(\vec{r},z,X)=q_1(r,z,X)(\vec{r}/r)$, where $q_1(r,z,X)$ is a scalar function of r. The symmetry condition (28) then implies: $q_1(r,z,X)=q_1(r,z,-X)$.

As far as the scalar functions are concerned, the symmetry relation $\varphi(\vec{r},X)=\varphi(-\vec{r},-X)$ implies simply $\varphi(r,X)=\varphi(r,-X)$ in the isotropic case. Thus

$$q_i(r,z,X) = q_i(r,z,-X), \quad i=2 \text{ and } 5$$

and

$$q_i(r,z,X) = -q_i(r,z,-X), \quad i=3 \text{ and } 4.$$

Simplifying, furthermore, $\nabla_{\vec{r}}[\varphi(r)\vec{r}/r]=r^{-1}(\partial/\partial r)(r\varphi)$ and using the notation

$$\tilde{q}_3(r,z,X) = k_0 q_4(r,z,X) - q_3(r,z,X),$$

we can finally write Eq. (24) as

$$\frac{1}{r}\frac{\partial}{\partial r} r[q_1(r,z,X)P(r,z,X)] + 2k_0\left\{\frac{\partial^2}{\partial X^2}[q_2(r,z,X)P(r,z,X)] - \frac{1}{r}\frac{\partial}{\partial r}\left[r\frac{\partial P}{\partial r}(r,z,X)\right]\right\} + \frac{\partial}{\partial X}[\tilde{q}_3(r,z,X)P(r,z,X)] + q_5(\vec{r},z,X)P(r,z,X) = 0. \qquad (29)$$

This equation is the evolution equation of the PDF's $P(r,z,X)$, through the scales r, in the assumption of isotropy restricted to a plane perpendicular to an axis z. Note here that the particular form of the operators gradient $\nabla_{\vec{r}}$ and Laplacian $\nabla_{\vec{r}}^2$ in the 2D isotropy hypothesis (polar coordinates) is different from their form obtained with the 3D isotropy hypothesis (written is spherical coordinates, as specified in Sec. II).

IV. CONDITIONAL EXPECTATIONS

The conditional expectations closing Eq. (29) are presented in the following figures for $R_\lambda=40$, with the Prandtl number $\mathrm{Pr}=1$ and the mean gradient $G=1$. Conditional expectations and PDF's necessary to test Eq. (29) were computed in a plane $\Pi\perp\vec{G}$ fixed $(z=cst)$. It was found that the results do not depend on the plane chosen, as expected from the overall homogeneity of the numerical flow. For this reason the results presented here were obtained by averaging over the entire computational domain, which greatly improved the quality of the statistics.

Equations (19) and (20) show that q_1 and q_2 are almost the same as those for the 3D isotropy theory which are presented in Fig. 1. In fact, q_1 is exactly the same, being associated with the velocity increments computed in a plane perpendicular to the mean gradient. The conditional expectation q_2 is here the horizontal squared temperature gradient conditioned by the temperature increment, thus it is proportional to the total squared temperature gradient

$$q_2 = \langle[(\nabla_x\theta)^2+(\nabla_y\theta)^2]/\Delta\theta\rangle = 0.85\times\tfrac{2}{3}\langle[(\nabla_x\theta)^2+(\nabla_y\theta)^2+(\nabla_z\theta)^2]/\Delta\theta\rangle.$$

This relation between the horizontal squared temperature gradient and the total squared temperature gradient emphasizes the fact that the mean temperature gradient $\vec{G}$ induces some anisotropy, the squared temperature gradient on the z direction being sensibly larger than those for the two other directions. The conditional expectations $\tilde{q}_3$ and q_5, involved in the new additional terms are plotted in Fig. 11.

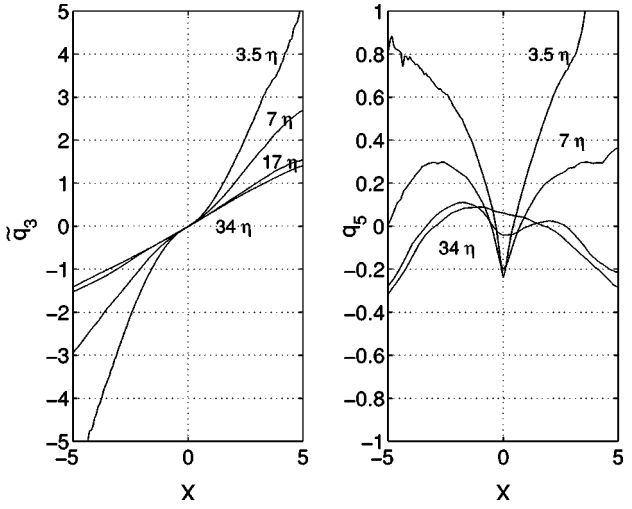

FIG. 11. Conditional expectations involved in Eq. (29), $\tilde{q}_3$ (left) and q_5 (right), for the scales 3.5η, 7η, 17η, and 34η.

In agreement with the theoretical constraints (28), q_3 and q_4 and thus also $\tilde{q}_3$ should be odd functions of X, whereas q_5 tends to be an even function. We carried out the same analysis for $R_\lambda = 70$, the results being qualitatively the same. The new conditional expectations take the anisotropy into account. Figure 11 shows that all effects are present even in the simple case of the DNS of a fully homogeneous and isotropic velocity turbulent field transporting a scalar with a mean gradient. In this case, the mean gradient is the only source of inhomogeneity and anisotropy so that the individual conditional expectations can be expected to be explicitly related to G.

Note here that, as was the case for the conditional expectations q_1 and q_2 used for the 3D approach, we could not derive so far any theoretical expression for these ''input data'' of the problem. The q_1 and q_2 conditional expectations were determined using either experimental or DNS data, as explained in Ref. [33]. Their behavior seems to be qualitatively universal, especially for the small scales, where both conditional expectations become symmetric. A first qualitative tentative attempt to explain the q_1 ''A'' shape was made in Ref. [28].

However, a theoretical calculation of these conditional expectations q_1 and q_2 should be done first of all in some simple flows. A velocity field generated by a Lundgren vortex [44] presents a relatively simple expression for all its components. It may thus be possible to introduce a scalar blob into this flow, and to pursue its time evolution analytically, while this blob is enhanced by the vortex, diffused, and finally completely dissipated. By knowing the velocity and temperature distributions in each point of the space, it would be possible to compute the different conditional statistics.

Concerning the five conditional expectations presented in this work, a similar analysis would be obviously very difficult, as q_3, q_4, and q_5 are indeed very specific of the mixing properties. Alternatively, an analysis of their symmetry properties was performed in Sec. III C. Here these conditional expectations are simply computed, as additional information about the mixing. Our present aim is mainly to affirm that 2D homogeneity and isotropy do influence the cascade on very small scales.

V. PLANAR ISOTROPY THEORY VALIDATION

A. Balance of the PDF equation

In this section we present how the additional terms accounting for anisotropy contribute to the total balance between the terms. We consider the two criteria retained in Sec. II: comparison of the balance of terms of Eq. (29) at $X=0$ and a modified Yaglom equation resulting from Eq. (29).

We write Eq. (29) in its dimensionless form, using the same reference variables as for Eq. (3) (see Ref. [33]): λ_θ, u', and θ'. The terms appearing in Eq. (29) will be numbered following the scheme: I+II−III+IV+V=0. The validity of the equation at $X=0$ will be tested by adding the two new terms to the terms I and II, and by comparing their sum to III.

The five terms are presented in Figs. 12 and 13 for the case $R_\lambda = 40$, Pr=1, and $G=1$.

The cancellation of the sum of all the terms of the equation is very well verified for all the values of X, as shown in Fig. 14 for the scales $r=15\eta$ and 35η.

The balance of individual terms for varying r at $X=0$ is represented in Fig. 15. The 2D isotropy equation is perfectly verified at all scales. The progress realized by our theory is directly measurable when comparing Figs. 15 and 3. A simi-

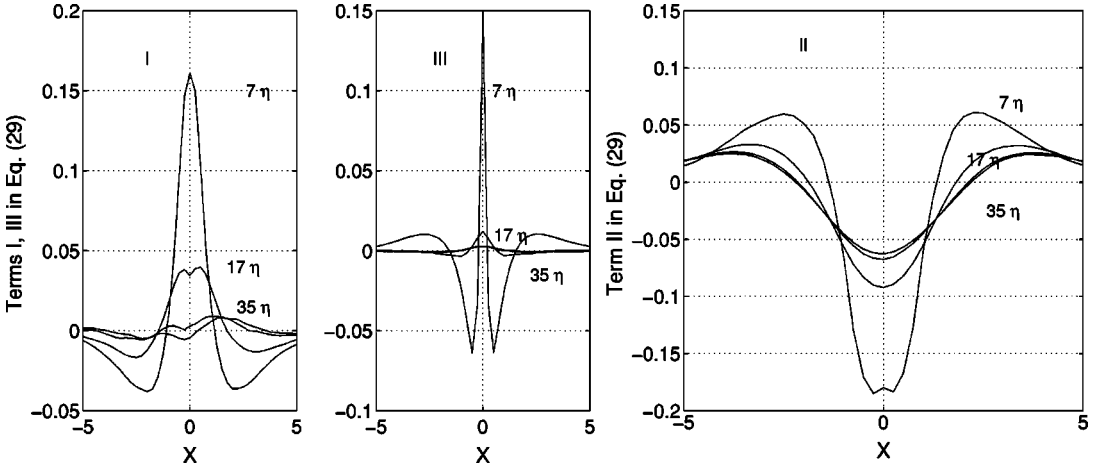

FIG. 12. The terms I, II, and III in Eq. (29), for $R_\lambda = 40$ and Pr=1.

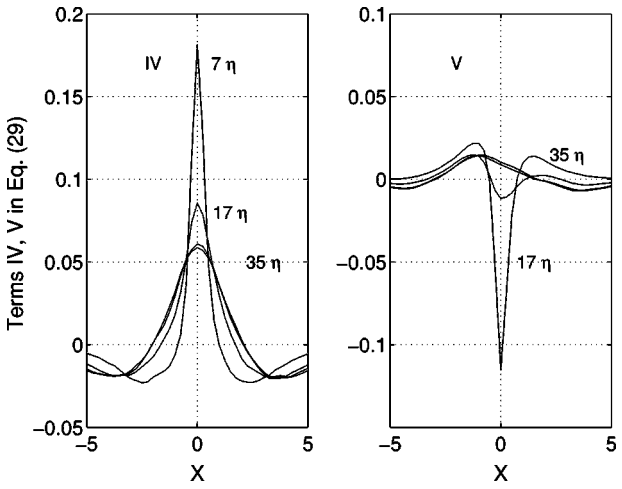

FIG. 13. The terms IV and V in Eq. (29), for $R_\lambda = 40$ and Pr=1.

lar agreement is obtained at $R_\lambda = 80$ (Fig. 16), except for the magnitude order of the different terms, which is approximately doubled for a doubled Pe number (0.4 in Fig. 16 to be compared with 0.2 in Fig. 15). Therefore, the evolution equation (29) is well balanced, and can be used to predict the evolution of the PDF's through the scales.

The modified Yaglom equation results from a multiplication by X^2 of both sides of Eq. (29), an integration over X, a multiplication by r, an integration (primitive calculus) with respect to r, and finally dividing the result by r. More specifically, we compute the averages over the plane Π as follows:

$$k_0\left\langle \frac{\partial^2 \Delta\theta}{\partial z^2}\,\Delta\theta \right\rangle - \left\langle u_z \frac{\partial \Delta\theta}{\partial z}\,\Delta\theta \right\rangle$$

$$\equiv \int_{-\infty}^{+\infty} [k_0 q_4(r,\Delta\theta) - q_3(r,\Delta\theta)]\Delta\theta P(r,\Delta\theta) d\Delta\theta$$

and

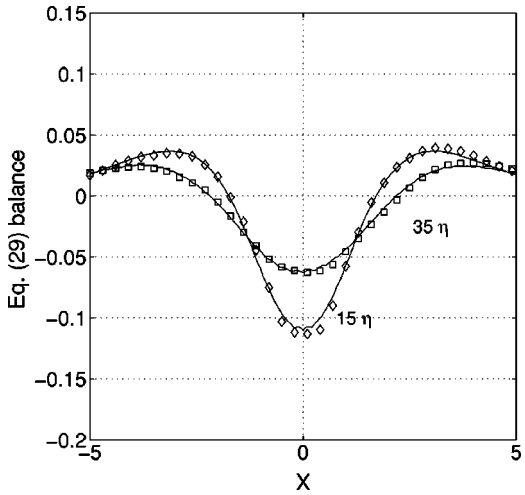

FIG. 14. Comparison between terms II (continuous line) and III−I−IV−V, for the scales 15η ($\diamond$) and 35η ($\square$), for $R_\lambda = 40$ and Pr=1.

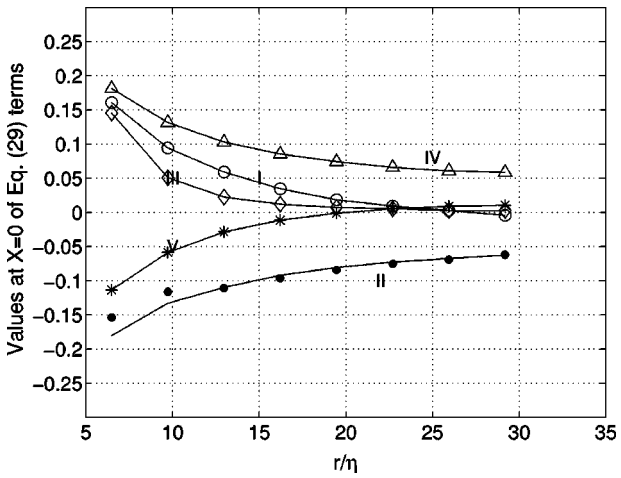

FIG. 15. Comparison between the values at $X=0$ of terms II (continuous line) and III−I−IV−V (●), for $R_\lambda = 40$ and Pr=1.

$$\left\langle \frac{\partial u_z}{\partial z}(\Delta\theta)^2 \right\rangle \equiv \frac{1}{2}\int_{-\infty}^{+\infty} q_5(r,\Delta\theta)(\Delta\theta)^2 P(r,\Delta\theta) d\Delta\theta,$$

using the conditional expectations, and the probability density function $P(r,\Delta\theta)$ of temperature increments $\Delta\theta$.

For simplicity, we further note that

$$m(r) \equiv k_0\left\langle \frac{\partial^2 \Delta\theta}{\partial z^2}\,\Delta\theta \right\rangle - \left\langle u_z \frac{\partial \Delta\theta}{\partial z}\,\Delta\theta \right\rangle$$

and

$$n(r) \equiv -\left\langle \frac{\partial u_z}{\partial z}(\Delta\theta)^2 \right\rangle.$$

We further obtain

$$-\langle \Delta u(\Delta\theta)^2\rangle + 2k_0 \frac{\partial}{\partial r}\langle(\Delta\theta)^2\rangle + \frac{2}{r}\int_0^r m(\tilde{r})\tilde{r}\, d\tilde{r}$$

$$+\frac{2}{r}\int_0^r n(\tilde{r})\tilde{r} d\tilde{r} = 2\overline{N}_p r, \tag{30}$$

where $\tilde{r}$ is a dummy variable, playing the role of the separation r, and $\overline{N}_p = k_0\langle(\nabla_x\theta)^2 + (\nabla_y\theta)^2\rangle$ is the passive scalar ''planar'' dissipation for temperature.

Using the conditional expectations presented in Sec. IV, we verify Eq. (30) for different cases, after having written the equation in its dimensionless form, under the form $A + B + D + E = C$, and keeping the same signification as in Eq. (4), for each of the terms. Here we present cases $R_\lambda = 40$ and Pr=1, but similar results are obtained for all the other cases, i.e., $R_\lambda = 40$, Pr=0.5; $R_\lambda = 70$, Pr=1; or $R_\lambda = 80$, Pr=1. Everywhere the agreement is very good and uniform throughout the scales.

The new term $D+E$ adds a positive contribution to the term $A+B$, which results in a very good compensation of the term C that could not be obtained by the 3D isotropy theory. This source term has the tendency to equilibrate the term C at a certain large scale, where effectively the advective term

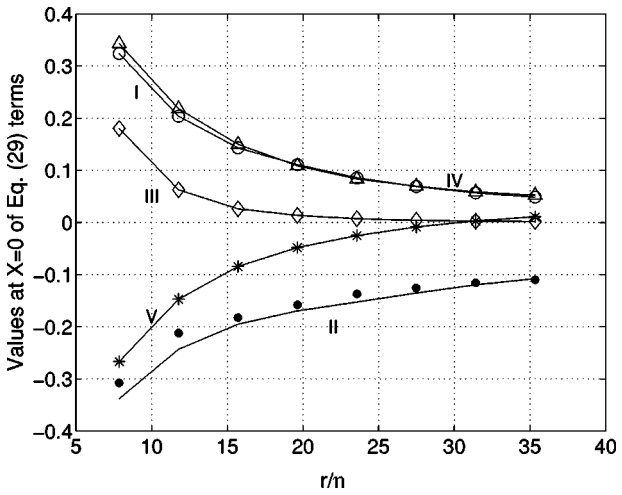

FIG. 16. Comparison between the values at $X=0$ of terms II (continuous line) and III$-$I$-$IV$-$V (●), for $R_\lambda=80$ and Pr=1.

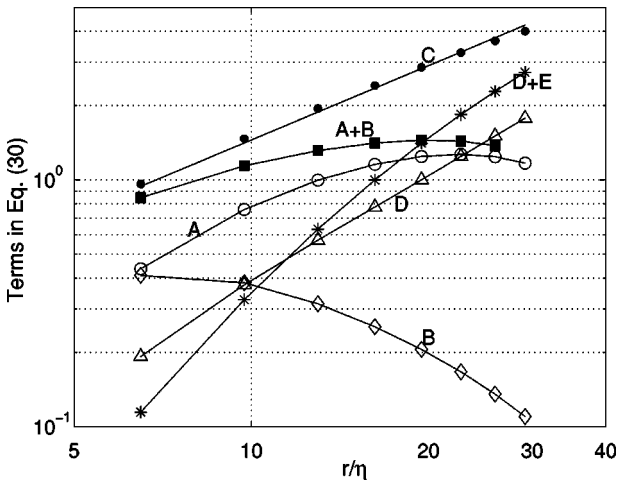

FIG. 17. Generalized Yaglom's equation verification, for $R_\lambda=40$ and Pr=1. The term $A+B$ (■) is the same as for the classical Yaglom equation. The new terms are D (△) and $D+E$ (*). $A+B+D+E$ (●) is to be compared with C (continuous line).

will be zero. The term E is simply the result of our hypothesis and of the calculation in the horizontal plane, but the most important term from the physical point of view is the term D, which is the expression of the mean gradient through the scales. As expected, its role decreases as one reaches smaller scales, but it is very important at large scales. The 2D isotropy and homogeneity assumptions thus apply perfectly to all scales for the investigated DNS of passive scalar mixing in a somewhat idealized configuration.

B. Prediction of the PDF evolution

In order to better emphasize the necessity of our approach which uses planar isotropy, we are now interested in investigating to what extent Eqs. (29) and (3) predict the intermittent behavior of the PDF's. In other words, what is the link between intermittency and the assumption of 3D isotropy or planar isotropy? Such a study was already performed in Refs. [32,33] for the equation supposing 3D isotropy and for relatively large Reynolds numbers. It was shown that, for small scales, this equation predicts the PDF evolution very well. We will now investigate this problem for $R_\lambda=40$, and Pr=1. At small Reynolds numbers, small and large scales do not decouple. Testing our approach at a small Reynolds number is therefore a stringent test. We perform the numerical integration of Eqs. (3) and (29), starting from an initial condition (the PDF and its r derivative at a large scale). The integration method is the same as in Ref. [33], i.e., an implicit scheme with a negative scale step: $\delta r=-0.001$. The conditional expectations at each scale are simply injected. The numerical integration is first performed for Eq. (3), starting from 17η, where this equation is relatively well verified (see Fig. 9 of the present paper). The PDF at 17η is not Gaussian, and it contains in a way some information about the large scales of the mixing. Figure 18 shows the numerical solution of Eq. (3) for the scales 7η and 3.5η, the smallest scale of the domain. These numerical solutions are compared with the real PDF's (dotted lines). Relatively good agreement is obtained for small scales, especially at $X=0$. Note also the ''specific'' shape of the Eq. (3) numerical solution: for relatively large X, this solution presents tails which are too abrupt in comparison with the real PDF's. The same behavior was obtained for other data; see Fig. 11 of Ref. [32] or Fig. 7 of Ref. [33].

We may conclude that Eq. (3) presents a ''predictability domain'' of $[3.5\eta-17\eta]$, since the PDF at 17η is able to lead to a realistic PDF at 3.5η, via this equation using 3D isotropy. Starting from a scale larger than 17η, a nonrealistic PDF is obtained, at any smaller scale.

Moreover, it could be noticed that the predictability domain of the PDF equation using 3D isotropy could be correlated with the aspect at $X=0$ of the conditional expectation q_1, which is directly related to the dynamic field. Figure 19 illustrates the $q_1(r,X=0)$ evolution, for two cases: Pe=82 and 40. Note here that the computational size is 110η for Pe=40, and 250η for Pe=82. Vertical arrows point to the largest scale of the predictability domain of equation 3: 35η for Pe=82 (see Ref. [33]), and 17η for Pe=40 (present work). Equation (3) seems to describe the evolution through

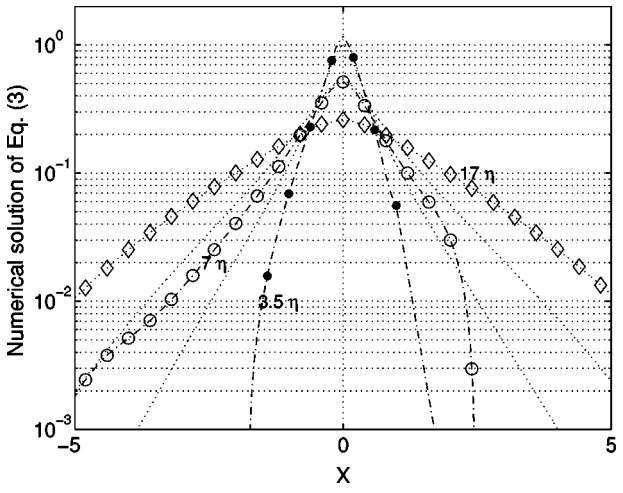

FIG. 18. Numerical solution of Eq. (3) ($R_\lambda=40$, Pr=1), for the scales 7η (○) and 3.5η (●). The initial condition is the PDF at 17η (◇) which is not a Gaussian. No symmetrization has been done.

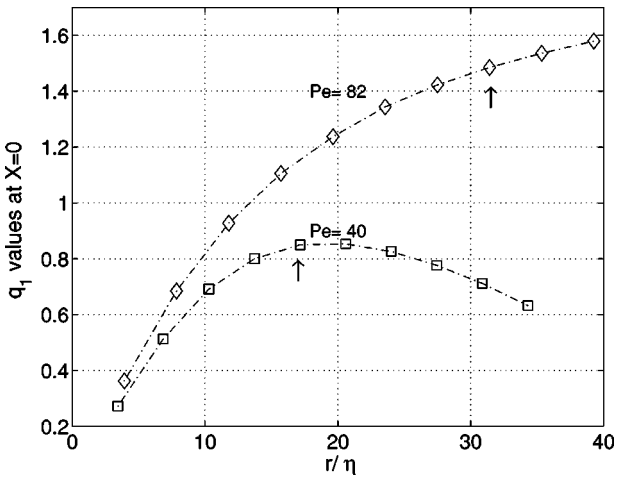

FIG. 19. $q_1(r,X=0)$ evolution for different Péclet numbers: Pe=82 ($\diamond$) and Pe=40 ($\square$).

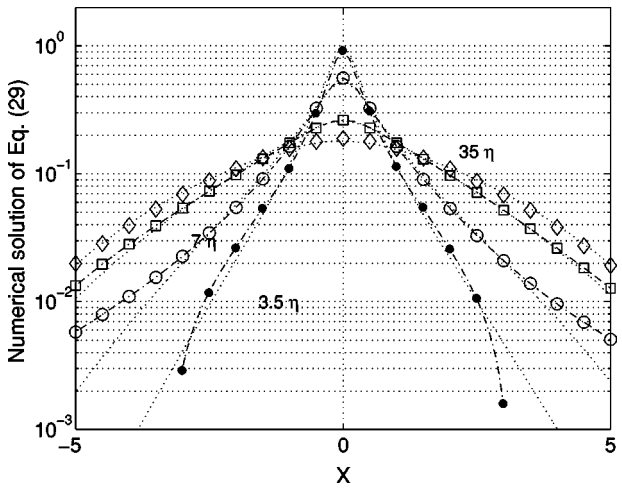

FIG. 20. Numerical solution of Eq. (29) ($R_\lambda=40$, Pr=1), for the scales 17η ($\square$), 7η ($\bigcirc$), and 3.5η ($\bullet$). The initial condition is the largest scale PDF ($\diamond$) which is quasi-Gaussian. Dotted lines represent real PDF's for the same scales. No symmetrization has been done.

scales of the PDF rather well, for the scales when $q_1(X=0)$ decays with r. These scales could be associated with a dissipative zone. However, more needs to be understood concerning the link between the behavior of the PDF equation and the conditional expectations, especially q_1.

As far as Eq. (29) is concerned, we showed that it is well balanced for different Pe numbers and for all scales, whereas Eq. (3) (using 3D isotropy) is not. This result proves that once 2D homogeneity and isotropy are correctly taken into account, a realistic PDF description can be deduced. This is a very useful result, since the equation using planar isotropy could be further considered as a tool to study intermittency in anisotropic and inhomogeneous turbulent mixing.

In Fig. 20, we show the numerical solution of Eq. (29), for the scales 17η, 7η, and 3.5η, which are to be compared with the real PDF's (dotted lines). Very good agreement is obtained for all the scales. Similar results are obtained for other Re numbers. The importance of this result consists in the fact that, starting from a large-scale PDF (in this case a quasi-Gaussian PDF), we can predict with good accuracy the PDF's until the very small scales of the domain.

The PDF at 3.5η in Fig. 18 is to be critically compared with the corresponding PDF (3.5η) in Fig. 20, and both of them with the real PDF. The value at the level of 10^{-2} of the real PDF at 3.5η is much better reproduced by the approach using planar isotropy, than by Eq. (3). The approach using 2D isotropy [Eq. (29)] leads to a numerically computed PDF closer to the real PDF. Also, the predictability domain covers all the scales of the domain. For Pe=40, the predictability domain of Eq. (3) is limited, whereas Eq. (29) does predict all the statistics starting from a large-scale PDF (at 35η). In particular, the intermittent behavior of the PDF is more correctly reproduced, through the equation obtained using 2D homogeneity and isotropy, and by taking into account some terms which are the direct expression of the mean temperature gradient influence.

VI. CONCLUSION

Internal intermittency of the passive scalar strongly influences the behavior of the PDF's of temperature increments, for the scales situated in the inertial and dissipative ranges. In order to understand, qualitatively and quantitatively, the evolution of the PDF shapes through the scales, we first investigate a previously obtained equation for the PDF evolution. The different terms of this equation, using 3D isotropy as a major hypothesis, are correctly balanced, for a range of scales which includes the dissipative zone and only a small part of the inertial zone. The equation validation domain depends on the Péclet number of the mixing.

In order to link the small scale to the large injection scales correctly, in a mixing created by a mean temperature gradient and a homogeneous, isotropic dynamic field, we relaxed the 3D isotropy to a 2D one, by separating the direction of the anisotropy, parallel to $\vec{G}$, from the plane perpendicular to $\vec{G}$, where 2D isotropy is supposed to hold. An equation is obtained, from which it is possible to obtain a generalized form of Yaglom's equation. Additional conditional expectations are thus involved; all these quantities are related to the particular geometry of the mixing and play an important role in the general balance of the equation. The DNS data analyzed herein show that the level of agreement and the range of scales where our prediction is valid are significantly enhanced when this equation is considered.

Therefore, the main result of the present paper is that a correct prediction of the statistics of the passive scalar increments at inertial and dissipative scales, smaller than the injection scale, is possible provided the large injection scales are properly taken into account, as it is done by the supplementary terms we calculated.

ACKNOWLEDGMENT

We acknowledge the support of DRET, under Contract Nos. 95/2592*A* and *B*, and of IDRIS for computer resources.

APPENDIX

We compute here the second term of Eq. (11):

$$\left\langle \frac{\partial^2 g}{\partial X^2}(\Delta\theta(\vec{x},\vec{r},t),\vec{r})[\nabla_{\vec{x}}\Delta\theta(\vec{x},\vec{r},t)]^2 \right\rangle(\vec{r},z)$$

$$= \lim_{R\to\infty}\frac{1}{\pi R^2}\int_{(x^2+y^2)<R^2}\frac{\partial^2 g}{\partial X^2}(\Delta\theta(\vec{x},\vec{r},t),\vec{r})[\nabla_{\vec{x}}\theta(\vec{x}+\vec{r},t)-\nabla_{\vec{x}}\theta(\vec{x},t)]^2 dx\,dy$$

$$= \lim_{R\to\infty}\frac{1}{\pi R^2}\left\{\int_{(x^2+y^2)<R^2}\frac{\partial^2 g}{\partial X^2}(\Delta\theta(\vec{x},\vec{r},t),\vec{r})[\nabla_{\vec{x}}\theta(\vec{x}+\vec{r},t)]^2 dx\,dy\right.$$

$$+\int_{(x^2+y^2)<R^2}\frac{\partial^2 g}{\partial X^2}(\Delta\theta(\vec{x},\vec{r},t),\vec{r})[\nabla_{\vec{x}}\theta(\vec{x},t)]^2 dx\,dy$$

$$\left.-2\int_{(x^2+y^2)<R^2}\frac{\partial^2 g}{\partial X^2}(\Delta\theta(\vec{x},\vec{r},t),\vec{r})\nabla_{\vec{x}}\theta(\vec{x}+\vec{r},t)\cdot\nabla_{\vec{x}}\theta(\vec{x},t)dx\,dy\right\}, \tag{A1}$$

where

$$\lim_{R\to\infty}\frac{1}{\pi R^2}\int_{(x^2+y^2)<R^2}\frac{\partial^2 g}{\partial X^2}(\Delta\theta(\vec{x},\vec{r},t),\vec{r})[\nabla_{\vec{x}}\theta(\vec{x}+\vec{r},t)]^2 dx\,dy$$

$$= \lim_{R\to\infty}\frac{1}{\pi R^2}\int_{(x^2+y^2)<R^2}\frac{\partial^2 g}{\partial X^2}(-\Delta\theta(\vec{x},-\vec{r},t),\vec{r})[\nabla_{\vec{x}}\theta(\vec{x},t)]^2 dx\,dy \tag{A2}$$

and

$$\lim_{R\to\infty}\frac{1}{\pi R^2}\int_{(x^2+y^2)<R^2}\frac{\partial^2 g}{\partial X^2}(\Delta\theta(\vec{x},\vec{r},t),\vec{r})\nabla_{\vec{x}}\theta(\vec{x}+\vec{r},t)\cdot\nabla_{\vec{x}}\theta(\vec{x},t)dx\,dy$$

$$= \lim_{R\to\infty}\frac{1}{\pi R^2}\int_{(x^2+y^2)<R^2}\frac{\partial^2 g}{\partial X^2}(\Delta\theta(\vec{x},\vec{r},t),\vec{r})\partial_z\theta(\vec{x}+\vec{r},t)\partial_z\theta(\vec{x},t)dx\,dy$$

$$+\lim_{R\to\infty}\frac{1}{\pi R^2}\left[\nabla_{\vec{r}}\int_{(x^2+y^2)<R^2}\frac{\partial g}{\partial X}(\Delta\theta(\vec{x},\vec{r},t),\vec{r})\nabla_{(x,y)}\theta(\vec{x},t)dx\,dy\right.$$

$$\left.-\int_{(x^2+y^2)<R^2}\frac{\partial\nabla_{\vec{r}}g}{\partial X}(\Delta\theta(\vec{x},\vec{r},t),\vec{r})\nabla_{(x,y)}\theta(\vec{x},t)dx\,dy\right], \tag{A3}$$

where $\nabla_{(x,y)}=(\partial_x,\partial_y)$ stands for the gradient operator in the (x,y) plane. In the last integral we use the identity

$$\nabla_{\vec{r}}\left[\frac{\partial g}{\partial X}(\Delta\theta(\vec{x},\vec{r},t),\vec{r})\right]=\frac{\partial^2 g}{\partial X^2}(\Delta\theta(\vec{x},\vec{r},t),\vec{r})\nabla_{(x,y)}\theta(\vec{x}+\vec{r},t)+\frac{\partial\nabla_{\vec{r}}g}{\partial X}(\Delta\theta(\vec{x},\vec{r},t),\vec{r}). \tag{A4}$$

The right-hand side of Eq. (A3) can then be written in the following way:

$$\lim_{R\to\infty}\frac{1}{\pi R^2}\int_{(x^2+y^2)<R^2}\frac{\partial^2 g}{\partial X^2}(\Delta\theta(\vec{x},\vec{r},t),\vec{r})\partial_z\theta(\vec{x}+\vec{r},t)\partial_z\theta(\vec{x},t)dx\,dy$$

$$+\lim_{R\to\infty}\frac{1}{\pi R^2}\left\{\nabla_{\vec{r}}\int_{(x^2+y^2)<R^2}\frac{\partial g}{\partial X}(\Delta\theta(\vec{x},\vec{r},t),\vec{r})\nabla_{(x,y)}\theta(\vec{x},t)dx\,dy\right.$$

$$+\int_{(x^2+y^2)<R^2}\nabla_{(x,y)}[\nabla_{\vec{r}}g(\Delta\theta(\vec{x},\vec{r},t),\vec{r})]dx\,dy$$

$$\left.-\nabla_{\vec{r}}\int_{(x^2+y^2)<R^2}\nabla_{\vec{r}}g(\Delta\theta(\vec{x},\vec{r},t),\vec{r})dx\,dy+\int_{(x^2+y^2)<R^2}\nabla^2_{\vec{r}}g(\Delta\theta(\vec{x},\vec{r},t)\vec{r})dx\,dy\right\}$$

$$=\lim_{R\to\infty}\frac{1}{\pi R^2}\int_{(x^2+y^2)<R^2}\frac{\partial^2 g}{\partial X^2}(\Delta\theta(\vec{x},\vec{r},t),\vec{r})\partial_z\theta(\vec{x}+\vec{r},t)\partial_z\theta(\vec{x},t)dx\,dy$$

$$+\lim_{R\to\infty}\frac{1}{\pi R^2}\nabla_{\vec{r}}\int_{(x^2+y^2)<R^2}\left[\frac{\partial g}{\partial X}(\Delta\theta(\vec{x},\vec{r},t),\vec{r})\nabla_{(x,y)}\theta(\vec{x},t)-\nabla_{\vec{r}}g(\Delta\theta(\vec{x},\vec{r},t),\vec{r})\right]dx\,dy$$

$$+\lim_{R\to\infty}\frac{1}{\pi R^2}\int_{(x^2+y^2)<R^2}\nabla^2_{\vec{r}}g(\Delta\theta(\vec{x},\vec{r},t),\vec{r})dx\,dy.$$

The term $\langle\nabla_{(x,y)}(\nabla_{\vec{r}}g(\Delta\theta(\vec{x},\vec{r},t),\vec{r}))\rangle$ is obviously equal to zero. As a result if we combine Eqs. (A1)–(A3) and the second term on the right-hand side of Eq. (10):

$$\left\langle\frac{\partial^2 g}{\partial X^2}(\Delta\theta(\vec{x},\vec{r},t),\vec{r})[\nabla_{\vec{x}}\Delta\theta(\vec{x},\vec{r},t)]^2\right\rangle(\vec{r},z)-\left\langle\frac{\partial^2 g}{\partial X^2}(\Delta\theta(\vec{x},\vec{r},t),\vec{r})[\partial_z\Delta\theta(\vec{x},\vec{r},t)]^2\right\rangle(\vec{r},z)$$

$$=\lim_{R\to\infty}\frac{1}{\pi R^2}\int_{(x^2+y^2)<R^2}\left[\left(\frac{\partial^2 g}{\partial X^2}(-\Delta\theta(\vec{x},-\vec{r},t),\vec{r})+\frac{\partial^2 g}{\partial X^2}(\Delta\theta(\vec{x},\vec{r},t),\vec{r})\right)[\nabla_{(x,y)}\theta(\vec{x},t)]^2\right.$$

$$\left.-2\nabla^2_{\vec{r}}g(\Delta\theta(\vec{x},\vec{r},t),\vec{r})\right]dx\,dy-2\lim_{R\to\infty}\frac{1}{\pi R^2}\nabla_{\vec{r}}$$

$$\times\int_{(x^2+y^2)<R^2}\left[\frac{\partial g}{\partial X}(\Delta\theta(\vec{x},\vec{r},t),\vec{r})\nabla_{(x,y)}\theta(\vec{x},t)dx\,dy-\nabla_{\vec{r}}g(\Delta\theta(\vec{x},\vec{r},t),\vec{r})\right]dx\,dy. \tag{A5}$$

[1] A. N. Kolmogorov, Dokl. Akad. Nauk SSSR **30**, 299 (1941).
[2] A. M. Oboukhov, Izv. Akad. Nauk SSSR Geogr. Geofiz. **13**, 58 (1949).
[3] S. Corrsin, J. Aeronaut. Sci. **16**, 757 (1949).
[4] F. Anselmet, Y. Gagne, E. J. Hopfinger, and R. A. Antonia, J. Fluid Mech. **140**, 163 (1984).
[5] A. N. Kolmogorov, J. Fluid Mech. **13**, 82 (1962).
[6] G. Parisi and U. Frisch, *Turbulence and Predictability in Geophysical Fluid Dynamics*, Proceedings of the International School of Physics ''E. Fermi,'' Course 84, edited by M. Ghil, R. Benzi, and G. Parisi (North-Holland, Amsterdam, 1985).
[7] U. Frisch, *Turbulence: the Legacy of A.N. Kolmogorov* (Cambridge University Press, Cambridge, 1995).
[8] B. Castaing, J. Phys. II **6**, 105 (1996).
[9] R. Friedrich and J. Peinke, Phys. Rev. Lett. **78**, 863 (1997).
[10] V. S. L'vov, E. Podivilov, and I. Procaccia, Phys. Rev. Lett. **79**, 2050 (1997).
[11] V. Yakhot, Phys. Rev. E **49**, 2887 (1994).
[12] R. A. Antonia, E. J. Hopfinger, Y. Gagne, and F. Anselmet, Phys. Rev. A **30**, 2704 (1984).
[13] C. W. Van Atta, Phys. Fluids **4**, 1803 (1971).
[14] B. Castaing, Physica D **73**, 31 (1994).
[15] Y. Zhu, R. A. Antonia, and I. Hosokawa, Phys. Fluids **7**, 1637 (1995).
[16] E. Lévêque, S. Ciliberto, C. Baudet, and G. Ruiz-Chavarria, in *Advances in Turbulence VII*, edited by U. Frisch (Kluwer Academic, Dordrecht, 1998), p. 573.
[17] G. He and B. Dubrulle J. Phys. II **7**, 793 (1997).
[18] R. H. Kraichnan, Phys. Fluids **11**, 945 (1968).
[19] R. H. Kraichnan, J. Fluid Mech. **64**, 737 (1974).
[20] R. H. Kraichnan, Phys. Rev. Lett. **72**, 1016 (1994).
[21] B. I. Shraiman and E. D. Siggia, Phys. Rev. E **49**, 2912 (1994).
[22] B. I. Shraiman and E. D. Siggia, C. R. Acad. Sci., Ser. II: Mec. Phys., Chim., Sci. Terre Univers **321**, 279 (1995).
[23] K. Gawedski and A. Kupiainen, Phys. Rev. Lett. **75**, 3834 (1995).

[24] M. Chertkov, G. Falkovich, I. Kolokolov, and V. Lebedev, Phys. Rev. E **52**, 4924 (1995).
[25] A. Pumir, Phys. Rev. E **57**, 2914 (1998).
[26] L. Mydlarski and Z. Warhaft, J. Fluid Mech. **358**, 135 (1998).
[27] Y. Jayesh and Z. Warhaft, Phys. Fluids A **4**, 2292 (1992).
[28] S. Vaienti, M. Ould-Rouis, F. Anselmet, and P. Le Gal, Physica D **73**, 99 (1994).
[29] M. Ould-Rouis, F. Anselmet, P. Le Gal, and S. Vaienti, Physica D **85**, 405 (1995).
[30] A. M. Yaglom, Dokl. Akad. Nauk SSSR **69**, 743 (1949).
[31] A. S. Monin and A. M. Yaglom, *Statistical Fluid Mechanics* (MIT Press, Cambridge, MA, 1975).
[32] L. Danaila, P. Le Gal, F. Anselmet, F. Plaza, and J. F. Pinton, Phys. Fluids **11**, 636 (1999).
[33] L. Danaila, F. Anselmet, P. Le Gal, J. Dusek, C. Brun, and A. Pumir, Phys. Rev. Lett. **79**, 4577 (1997).
[34] P. Mestayer, J. Fluid Mech. **125**, 475 (1982).
[35] K. R. Sreenivasan Proc. R. Soc. London, Ser. A **434**, 165 (1991).
[36] M. Holzer and E. D. Siggia, Phys. Fluids **6**, 1820 (1994).
[37] A. Pumir, Phys. Fluids **6**, 2118 (1994).
[38] C. Tong and Z. Warhaft, Phys. Fluids **6**, 2165 (1994).
[39] R. A. Antonia and C. W. Van Atta, J. Fluid Mech. **84**, 561 (1978).
[40] R. A. Antonia, F. Anselmet, and A. J. Chambers, J. Fluid Mech. **163**, 365 (1986).
[41] L. Danaila, F. Anselmet, T. Zhou, and R. A. Antonia, J. Fluid Mech. **391**, 359 (1999).
[42] Y. A. Sinai and V. Yakhot, Phys. Rev. Lett. **63**, 1962 (1989).
[43] R. A. Antonia, A. J. Chambers, and L. W. B. Browne, Exp. Fluids **1**, 213 (1983).
[44] T. S. Lundgren, Phys. Fluids A **5**, 1472 (1993).